



# Electrical resistivity and refraction seismic tomography in the detection of near-surface Qadimah Fault in Thuwal-Rabigh area, Saudi Arabia

Hamad H. AlQahtani<sup>1</sup> · Mohammed S. Fnais<sup>2</sup> · Sattam A. Almadani<sup>2</sup> · Mansour S. Alhumimidi<sup>1</sup> · Kamal Abdelrahman<sup>2,3</sup>

Received: 27 November 2019 / Accepted: 3 June 2021  
© Saudi Society for Geosciences 2021

## Abstract

Integrated geophysical data provides a powerful tool for subsurface imaging with reasonable accuracy. The 2-D electric resistivity tomography and seismic refraction tomography profiling are carried out at four sites in Thuwal-Rabigh area, west-central Saudi Arabia. These profiles oriented perpendicular to the proposed strike of the Qadimah fault to detect the Qadimah fault. The results indicate the presence of the Qadimah fault underneath the northern two profiles at shallow depths, while not recorded through the southern two profiles indicating the absence of fault or changing in its strike southward. These results confirmed the passing of Qadimah fault through the King Abdullah Economic City. The study displayed the extension of the fault through King Abdullah Economic City warning serious hazards in the future in case of reactivating the movement along the fault plane, especially the area has a noticeable seismic activity. Continuous monitoring of earthquake activities and displacement along the fault plane through installation local earthquake monitoring network equipped by global positioning system are highly recommended.

**Keywords** Electric resistivity tomography; · Seismic refraction tomography; · Qadimah fault; · Saudi Arabia

## Introduction

The Qadimah fault is discovered recently and extends parallel to the Red Sea coast to the north of Jeddah city. This normal fault was originated as a result of the Arabian tectonic plate margin gravity collapse following the opening of the Red Sea ~30 Ma (Roobol and Kadi 2008). This fault has been traced for a distance of 25 km via a 4-km high eroded fault scarp that comprises the first 10 km of this distance. However, it remains blurred if the fault is still active and poses a significant hazard to the area (Roobol and Kadi 2008).

Few geophysical inquiries have been carried out through the Thuwal-Rabigh area where AlTawash (2011) and Mahmoud (2012) conducted research and confirmed the presence of the fault with a small segment that traced by Roobol and Kadi (2008). They suggested that fault movements could have happened over the past several tens of thousands of years, which therefore represent a potential hazard for the area. However, the mechanism that generated the fault is still uncertain. One theory indicates this fault originated from the continued extension and rotation of a buried fault block, which would represent a seismic hazard to the city since it is likely that these blocks extend deep into the seismogenic zone (Roobol and Kadi 2008). Besides, it is indistinct whether the coastal strip is under a continued extension due to continental rifting that gives way to oceanic spreading following the presence of sufficient crustal stretching. Under this scenario, passive margins would usually form on either side of a rift where relatively little seismic activity occurs (Fossen 2010).

Several authors have detected subsurface faults in other areas using seismic refraction tomography (SRT) (e.g., Hanafy et al. 2012; Rezaei 2016; Rinaldi et al. 2019) as well as electric resistivity tomography (ERT) (e.g., Park and Wernicke 2003; Giocoli et al. 2008; Zhu et al. 2009; Ammar and Kamal 2018; Rizzo et al. 2019). These techniques applied to detect the Qadimah fault

Responsible Editor: Narasimman Sundararajan

✉ Kamal Abdelrahman  
khassanein@ksu.edu.sa

<sup>1</sup> National Center for Mining Technology, King Abdulaziz City for Science and Technology, P.O. Box 6086, Riyadh 11442, Saudi Arabia

<sup>2</sup> Department of Geology & Geophysics, College of Science, King Saud University, P.O. Box 2455, Riyadh 11451, Saudi Arabia

<sup>3</sup> Seismology Department, National Research Institute of Astronomy and Geophysics, Cairo, Egypt

in Thuwal-Rabigh area that situated to the north of Jeddah city along the coastal plain of the Red Sea between  $22.34^{\circ}$ – $22.52^{\circ}$  N and  $39.21^{\circ}$ – $39.23^{\circ}$  E (Fig. 1). This area includes two of the utmost strategic projects as King Abdullah Economic City and King Abdullah University of Science and Technology (KAUST). Based on the geological investigation, the Qadimah fault runs close to KAUST and the identifying of the fault strike is very important for seismic hazard assessment and risk mitigation of the region through the use of a joint interpretation of SRT and ERT, which were conducted to detect the fault and its associated subsidiary structures northward of the Thuwal-Rabigh area, as previously studied by AlTawash (2011) and Mahmoud (2012).

## Geological setting

The study area is located along the Red Sea within the Tihamat al Hijaz coastal plain. The region is largely covered by un lithified material of Quaternary age; farther inland,

alluvial gravels in wadi (i.e. ephemeral river bed) systems are of a similar age, as deposits in pans on the lava fields. These deposits can be subdivided into the following units (Fig. 1): reef limestone (Qc), which is the oldest and outcrops in a strip along the coast; sabkhah deposits (i.e., saline mud flats) (Qs); alluvial terraces and fans (Qu) that generally have an intricate, shallow, dendritic drainage system; alluvial and deluvial gravels and sands (Qal), which are the most recent deposits whereby the former fills the bottoms of wadis and the latter was formed in situ by weathering of plutonic masses; windblown sand (Qe) that covers some areas of Qu in a thin veneer and is also banked up against rocky hills as well as being accumulated in small dune fields.

Large areas of the coastal plain are covered by Qu, which range from thin veneers to several meters thick. Sediments occur inland at the foot of mountains and gravel terraces are present in most major wadi systems. The coarsest gravels that comprise the unconsolidated deposits are poorly sorted and

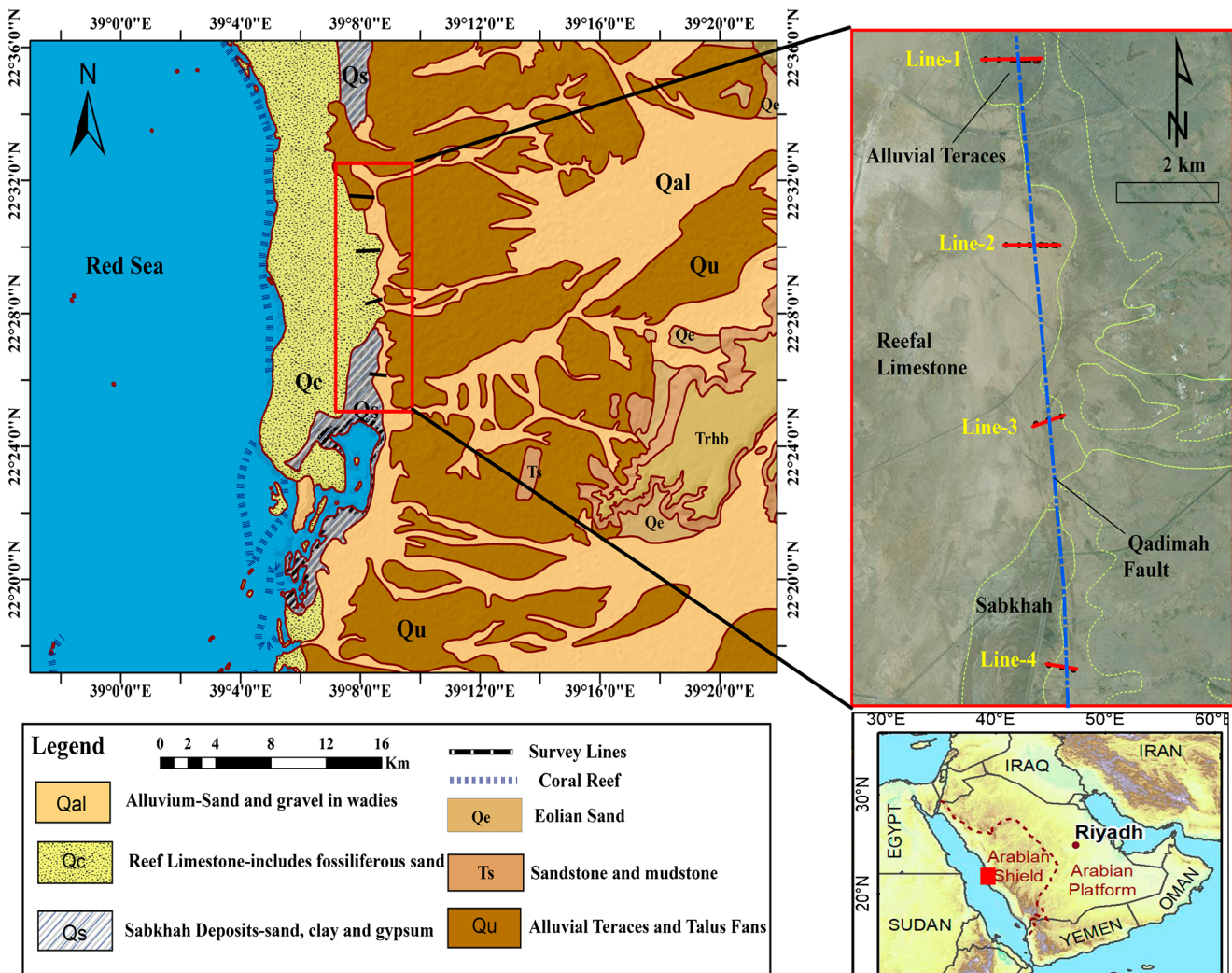


Fig. 1 Location map and geological setting of the study area

contain a high proportion of cobbles and boulders with diameters of ~20 cm or more. Many such clasts are probably residual deposits formed by disaggregation of the underlying Tertiary sedimentary rocks. The next coarsest gravels are also poorly sorted and contain numerous cobbles with diameters ranging from 10–20 cm. These occur as terrace gravels in many of the main wadis and as mountain pediments. Better-sorted gravels that include pebbles and cobbles mostly ranging from 5 to 10 cm are widespread in the study area.

Qc is exposed in a discontinuous belt along the Red Sea beach, and typically forms flat reef platforms that are a few hundred meters in length on the seaward side. Through area of study, the Qc is elevated 2–4 m above mean sea level and forms flat ground that is covered by Qs. Limestone is composed of abundant corals, lamellibranches, and gastropods that are cemented together but barely lithified, such that the rock is cavernous and very porous. Drilling has indicated that the limestone varies in thickness from 4 m to > 14 m, with the average being ~9.4 m (Moore and Al-Rehaili (1989)). The thickness gradually increases from east to west. C<sup>14</sup> dating has yielded an age of 40 000 years for samples collected from near the desalination plant northwest of Jeddah.

Several low-lying Qs occur immediately behind the coast. These are composed of brown terrigenous sands and clays, and generally have a salty crust with a white layer of salt ~0.5 cm thick in minor depressions. Sediments beneath the crust are moist and contain widespread interstitial gypsum. Towards the back of the Qs, crystals of anhydrite and selenite are present (Skipwith 1973). For several hundred meters inland from the shore, the Qs are covered by a thin, active algal mat, which binds the surface against deflation and also forms a relatively impervious layer that slows capillary evaporation and allows evaporate minerals to crystallize.

Long areas extend along the coastal plain strip are covered by Qe. The sand often accumulates into long, low (< 1 m high) ridges that are directed parallel to the prevailing wind (i.e., they are oriented approximately southeast). Much higher sand ridges (up to 10 m) have developed in places on the lee side of hills in the Tihamat al Hijaz coastal plain.

Qa1 that are generated in wadis are wide-spread along the coastal strip, and stretch seawards of the major wadi systems and filling low-lying areas. Alluvial gravels are largely confined to wadi channels that cross the coastal plain, while alluvial sands are deposited on neighboring flood plains and have commonly been reworked by the wind. Inland from the Tihamat Al Hijaz coastal strip, the alluvial sediments that fill the wadis contain a higher proportion of coarse material and composed of unconsolidated and poorly consolidated sands and gravels. In the lower spreads of the main wadis, alluvial sediments reach depths of the order of 15 m, whereas the alluvium is rarely more than 5 m thick in minor tributary wadis.

## Data acquisition

Four lines were suggested extend perpendicular to the expected northern expansion of the Qadimah fault (Fig. 1). Each of lines 1 and 2 includes 2 ERT profiles and one SRT profile. Before starting the field work and data collection, the work procedure was suggested that the electrical resistivity tomographic (ERT) profiles must be overlapped each other with certain distance, then the exact location of seismic refraction tomographic (SRT) profile will be selected later where it will cover the ERT segment that appears the trace of the fault. Then, repeating same procedure for the other surveying lines. Each of ERT profile extends with a total length of 475 m and overlapped with the second profile overlapped by 10 m. While third and fourth lines were only used for ERT. Two SRT profiles were carried out as well to outline the detailed sub-surface geological features near the fault. Field measurements and data collected were performed in the period of February - March 2016. The suggested sites of the studied profiles were selected crossing to the possible strike of the Qadimah fault (Roobol and Kadi 2008).

## Seismic refraction tomography (SRT)

Two of 2-D geoseismic profiles perpendicular to the expected path of the Qadimah fault scarp. The field acquisition parameters of SRT measurements are described in Table 1. Each profile was conducted on three sequential spreads with an overlap of 10 meters. For the first spread, seismic data were collected using an array of 24 vertical geophones of 4.5 Hz with a 5 m geophone spacing to form a total segment length of 115 m. The total spread was then moved forward where refraction data were gathered along the second spread with an overlap of the last 10 m of the first spread. The array was subsequently shifted into the third spread and data were again

**Table 1** Parameters of seismic tomographic field survey

Parameter	Description
Profile total length	345 m
Geophone interval	5 m
Source type	100 kg weight drop
Sample interval	125 $\mu$ s
Number of stacks	25 - 40
Total Record Length	256 ms
Acquisition Filter	Out - Out
Geophone Type	4.5 Hz
Number of Geophones	72
Number of Shot-points	72
Shot-points Interval	5 m
Seismograph model	Geode ( <a href="https://www.geometrics.com">Geometrics.com</a> )

collected with an overlay of the last 10 m of the second spread. Then, these three spreads were combined where the total length of the combined surveying spreads was 345 m. Similarly, the same process was repeated along the second profile. The seismic energy source was 100 kg-weight drop (WD) which produces seismic waves by the shock of 100 kg dropped on the striker plate on the ground surface. WD systems make use of simple crossbow technology to store the energy output from a gasoline-powered hydraulic system over ~8 s, and then release the energy into the ground when the hammer (100 Kg) impacts a plate at the ground surface. The energy output is of a high frequency was repeated such that stacking or vertical summation can occur.

For both profiles, the weight drop struck a 5-cm thick aluminum plate at each geophone location; each shot stacked number of times (generally, varies from 25 to 40) at the same shot-point to enhance the signal-to-noise ratio (SNR). Seismic traces were recorded using a 24-channel geometrics data recorder (Geode model), and the acquired areas were collected using out-out as a frequency band filter.

### Electrical resistivity tomography (ERT)

Six electrical resistivity profiles were surveyed at four locations (where each of lines 1 and 2 includes 2 profiles, while the other two profiles were conducted at 2 different locations) to perceive the sharp trace of the fault using a 2D resistivity survey line with Wenner resistivity configuration. The northern two ERT lines includes two of ERT profiles with overlapping distance between them. These profiles were surveyed along the same track of the 2D the northern seismic profiles to authenticate the subsurface variation in the soil resistivity. While the southern two ERT profiles were distributed at two different sites along the expected southern extension of the fault. The resistivity surveys in the present study were conducted using 96 metal electrodes spaced at 5 m intervals to form a total line length of 475 m. The parameters of ERT field measurements are described in Table 2.

The external power source used in our study was a 12-V battery that included a 12–800 V DC booster to provide the required high voltage. Data were recorded during the field investigation with Syscal-Pro resistivity meter (IRIS instruments). The meter includes a Syscal Pro Switch unit that is

designed for high productivity surveys, and uses segments of a multi-core cable. The Syscal Pro Switch 96 with 5 m interval consists of 4 segments of cable (a, b, c, and d) that each have 18 electrodes, which giving 475 m total of line length. The Syscal Pro meter is placed at the central point of the profile (i.e., between segments b and c).

## Data processing

### Electrical resistivity tomography (ERT)

The 2-D resistivity field data was downloaded from the Syscal Pro unit for processing and checked the quality. Then, transforming of the apparent resistivity into true resistivity was carried out through processing software by applying backward and forward modeling inversion processes. The output resistivity tomogram was a vertical geoelectric sections of the apparent resistivity below the electrode array. The following steps describe the stages involved in the processing operation: 1) The raw data is uploaded for processing and filtering. Once a data file is open in the master window, the data can be filtered and then converted into absolute resistivity ( $\rho$ ) values. Data points are examined for those of poor quality (i.e., data points that have either too high or too low apparent resistivity values), which are subsequently removed as necessary; 2) the filtered data are exported for further editing and removal of poor data points that have erroneous resistivity values (i.e., they appear to have either too high or too low resistivity values in comparison to neighboring data points); 3) the filtered data are subjected to the least-squares inversion routine and the output file produced by the inversion subroutine displays the measured apparent resistivity pseudo-sections and the model sections.

The produced 2D resistivity profiles include 650 data points of apparent resistivity values. These values contained some clear outlier points that were filtered out of the original dataset in preparation for the inversion process because outliers can affect the inversion result and can produce a distorted subsurface resistivity. The resultant 2D resistivity tomogram appears the subsurface variation of resistivity across a traverse. It is noted that, during data processing, it is vital that the root-mean-square error (RMSE) remains low as possible (Loke 1999) to achieve a good quality geologic model.

### Seismic refraction tomography (SRT)

Several researchers have been applied the traveltimes tomography to reconstruct the earth's subsurface velocity model based on the picked first arrival travel times (Aldridge and Oldenburg 1993; Ammon and Vidale 1993; Nolet 1987; Nemeth et al. 1997; Lutter et al. 1990). The procedure includes a finite difference (FD) solution to the eikonal equation

**Table 2** Parameters of the electric resistivity tomography (ERT) field survey

Parameter	Description
Resistivitymeter system	Syscal Pro
Array configuration	Wenner
Number of electrodes	96
Electrode interval	5m
Total profile length	475 m

(Qin et al. 1992), and Simultaneous Iterative Reconstructive Technique (SIRT) algorithm (Gilbert 1972) as well. The first stage is to assess the initial velocity model for the data using the offset-time (x-t) slope from the first arrivals in the seismograms. The initial velocity is iteratively readapted until the computed traveltimes match the observed traveltimes to achieve a specified accuracy in predicted traveltimes. A FD solution to the eikonal equation (Qin et al. 1992) is used to compute the predicted traveltimes used for calculating the traveltime residual, i.e., the difference between the observed and predicted traveltimes: These residuals are squared and summed together to get the data misfit function.

$$\epsilon = \frac{1}{2} \sum_i (t_i^{obs} - t_i^{cal})^2 \quad (1)$$

where the summation is over all the  $i_{th}$  raypaths in the velocity model,  $t_{is}^{obs}$  is the picked first arrival traveltime from the seismograms, and  $t_i^{cal}$  is the calculated traveltime from the eikonal equation.

The  $j$ th gradient of the misfit function  $\epsilon$  is given by:

$$\gamma_j = \frac{\delta \epsilon}{\delta s_j} = \sum_i \delta t_i \frac{\delta t_i}{\delta s_j}, \quad (2)$$

$$\text{where } \frac{\delta t_i}{\delta s_j} = l_{ij}; \gamma_j = \sum_i \delta t_i l_{ij} \quad (3)$$

where  $\delta t_i$  is the residual traveltime of the original misfit function,  $\delta s_j$  is the slowness perturbation in the  $j_{th}$  cell and  $l_{ij}$  is the length of the ray that visits the  $i_{th}$  cell. Finally, the

slowness model is updated iteratively by optimizing the gradient of the misfit function (using the steepest descent method etc.) and the slowness model update formula is given by:

$$s_j^{k+1} = s_j^k - \alpha \gamma_j \quad (4)$$

where  $\alpha$  is the step length and  $s_j^k$  is the slowness at the  $k_{th}$  iteration.

The first arrival traveltimes are picked for 5184 traces in both of the first and second 2D seismic profiles. A gathering shot from the second 2D seismic profile along with the first arrival traveltime picks (indicated by the green line) are shown in Fig. 2 (a, b, and c). Then, the elevation values for both profiles were used in the traveltime tomography method to account for topography changes along the profile. This correction undertakes that the data were collected on a straight datum line. This Pickwin software uses the ray tracing technique to interactively match the interpreted subsurface model to field data. The obtained traveltime-distance curves are illustrated in Fig. 3 (a, b, and c). These curves were subsequently used to obtain the subsurface layers and velocities using Plotrefa software.

## Results and discussion

The Qadimah fault was detected in both of the first and second lines while it was not recorded in the third and fourth lines. Therefore, the data of the third and fourth lines were excluded from the results while the results of the first and second lines

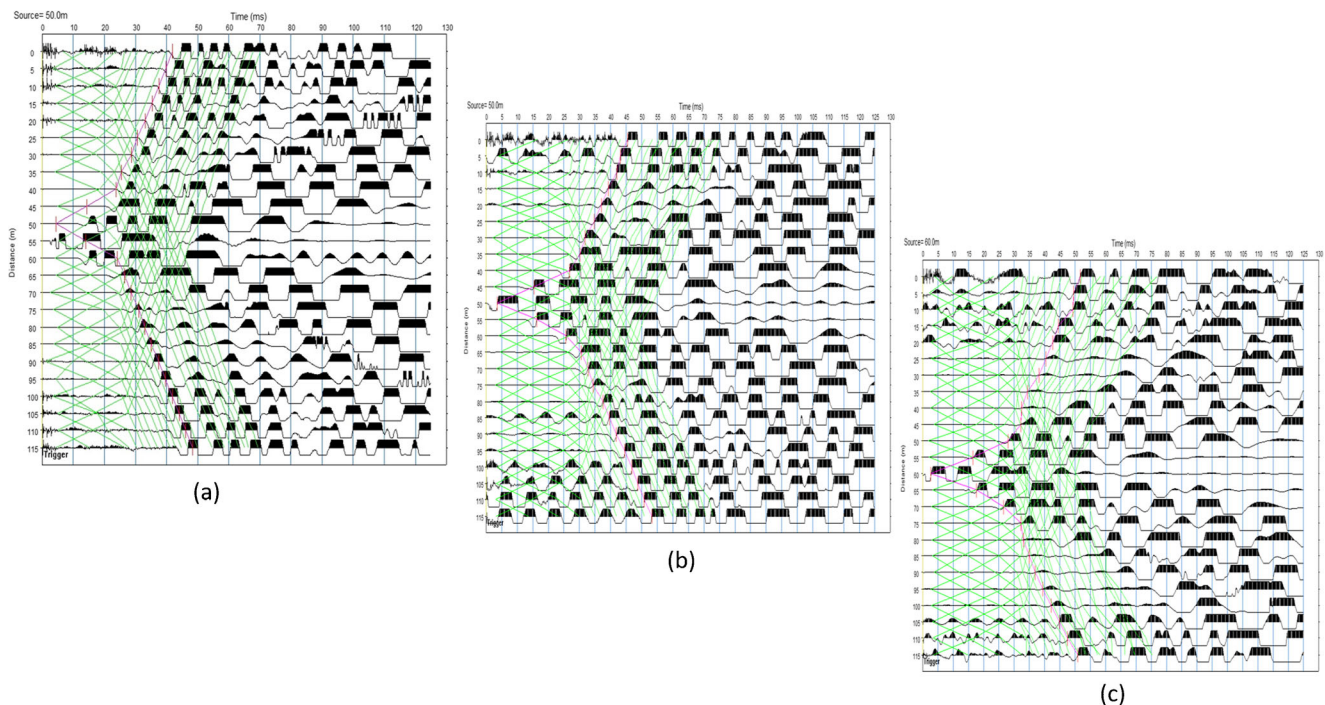


**Fig. 2** First break picking: a) for midpoint shooting the first spread in the line-1. b) for the midpoint shooting of the second spread in the line-1, and c) for the midpoint shooting of third spread in line-1

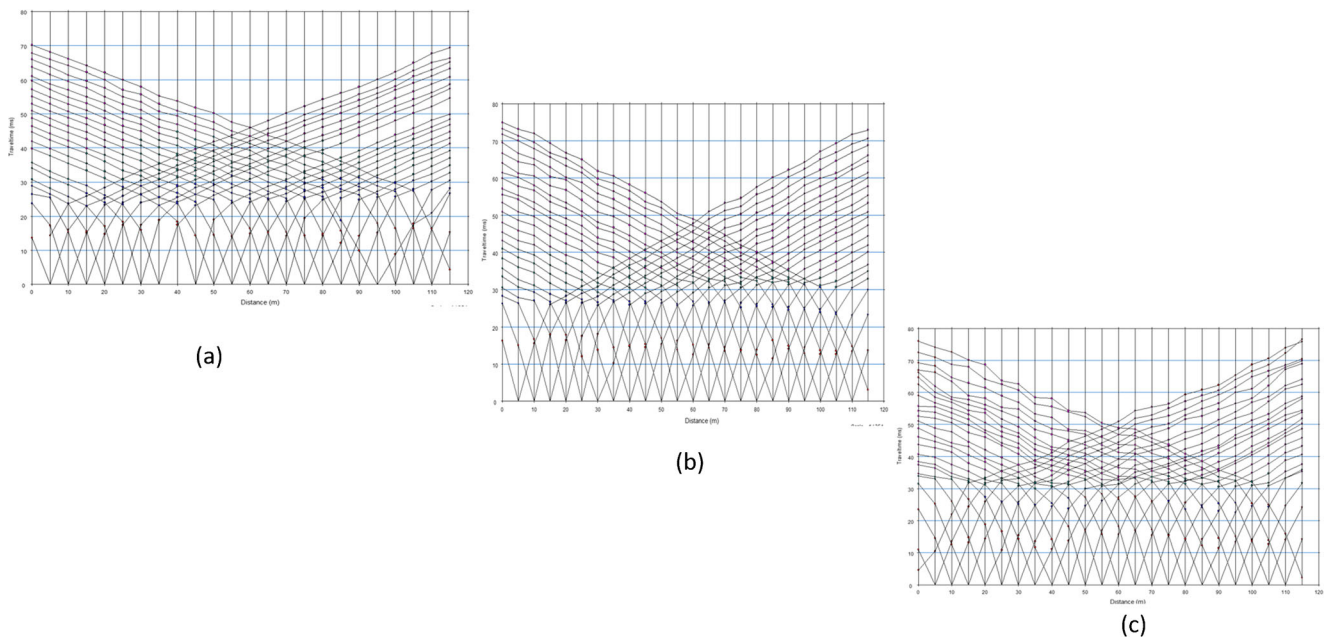


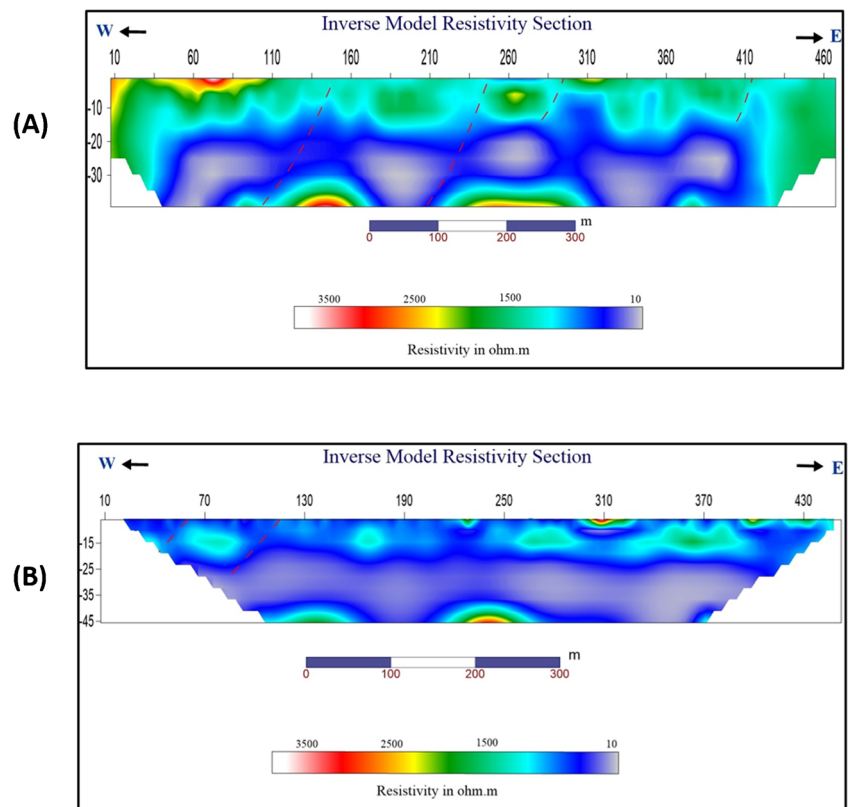
**Fig. 3** The traveltime-distance curve; a) for the first spread in the line-1; b) for the second spread in the profile No. 1, and c) for the third spread in line-1

have been discussed only. The 2D resistivity images and the 2D seismic tomography results are constructed for the Qadimah fault data (Figs. 4, 5, 6).

For 2D resistivity profiles, through the first profile, the apparent resistivity values reduced to 619 data points and 31 were eliminated due to their relatively high values, which

could affect the inversion results. While, the remaining apparent resistivity varies from 10 to 3500 ohm-m, and which, inverted to get the true resistivity changing of the subsurface. The logarithmic values of the final resistivity distribution are calculated and displayed in Fig. 4a. The logarithmic resistivity values were displayed instead of the true resistivity values

**Fig. 4** The interpreted 2D inversion resistivity model; a) for profile 1, while b) for profile 2



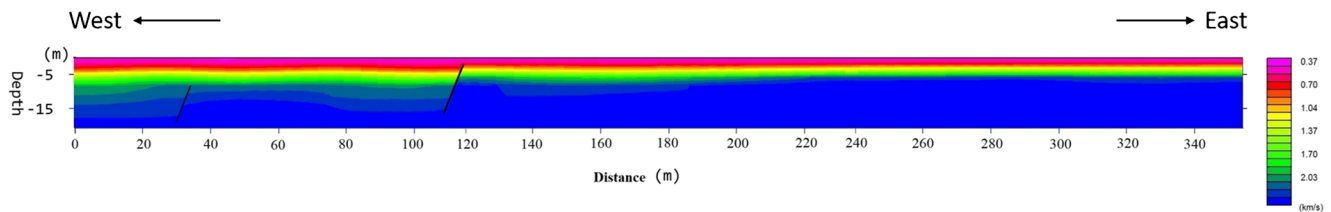


Fig. 5 P-wave 2D velocity- depth tomogram of line 1

because the inversion process produces a result with a wide variation of resistivity values, and the logarithmic plot compresses the range of resistivity values in the model.

Figure 4a illustrates wide range of resistivities which, in turn, expresses different lithology where it ranges from 10 to 35000 ohm-m. According to several studies, the resistivity values less than 50 ohm-m represents loose sediments accumulated with saline water. These very low resistivity anomalies or salt rollers appears well with 20–40 m depth. These salt rollers affected by the Qadimah fault, while resistivities vary from 50 to 1000 ohm-m exhibit Quaternary sabkhah deposits (Qs) which prevails in the fault area. These sabkhah sediments were formed may be due the normal fault movements tilted the seaward block, resulting a shallow lagoon forming along the fault scarp (Roobol and Kadi 2008). In addition, the higher resistivities from 1000 to 2400 ohm-m represents the Quaternary limestone, reef facies (Qc). These emerged coral reefs form a narrow zone of 1–3 m high sea cliff along the coastline and extends inland several kilometers with an elevation around 5 to 6 m along the northern end of the Qadimah fault, mostly under a cap of terrace deposits (Roobol and Kadi 2008). The higher resistivities greater than 2400 ohm-m shown as localized areas that may be represents terraces or cap of very hard deposits of emerged reefs.

Similarly, for the second profile the acquired apparent resistivity values were reduced to 623 values. The remaining resistivity values ranging from (10–3500 ohm-m) were inverted as well to get the true resistivity model of the subsurface. The logarithmic values of the final resistivity distribution are displayed in the tomogram shown in Fig. 4b. This figures show the same features of the first profile where the very low

resistivities appear between 20 and 35 m depth. Sabkhah deposits with resistivity ranges from 50 to 1000 ohm-m include the entire geoelectric section. But the Quaternary limestone with resistivity values from 1000 to 2400 ohm-m exhibits disconnected blocks down to 15 meters depth. While the higher resistivity anomalies appears at separate sites representing very hard deposits of emerged reefs.

For 2D seismic tomography, the resulting velocity tomogram for the first 2D seismic profile is displayed in Fig. 5, where values of seismic velocity are indicated in the form of contour lines with increasing depth along profile. The maximum depth reached was 20 m while the velocity ranges between 370 m/s and 2030 m/s. The strike of the Qadimah normal fault traced at 120m from the starting point of the profile where the vertical displacement reaches about 1.5 m where the fault block tilted westward. Another fault has been traced at distance of 30 m from the start of this profile. It is affected the deeper layer than that of the main Qadimah fault. Moreover, Fig. 6 illustrates 2D seismic tomogram of the second 2D seismic profile. The depth of this tomogram reaches 55 m while the P-wave velocity ranges from 550 to 1780 m/s. It is noticed that the penetrated depth of this profile is less than that of the first profile which, in turn, reflects materials with less density or loose sediments saturated with saline water. In this profile, the trace of the Qadimah fault has been detected at distance 150 m from the starting point of this profile even the amount of displacement is less than that of the first profile that may be due to the presence of salt zone. Another fault has been identified at distance of 270 m from the beginning of this profile with very small amount of displacement.

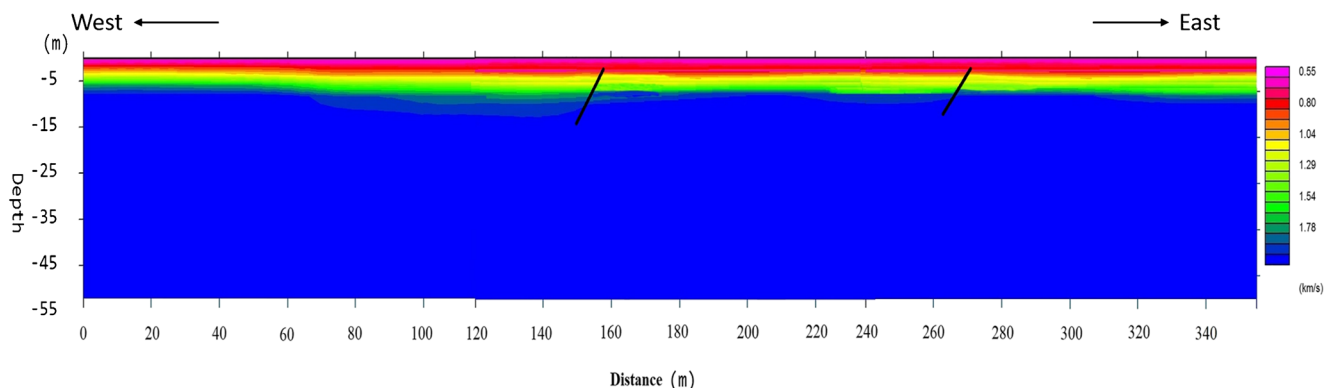
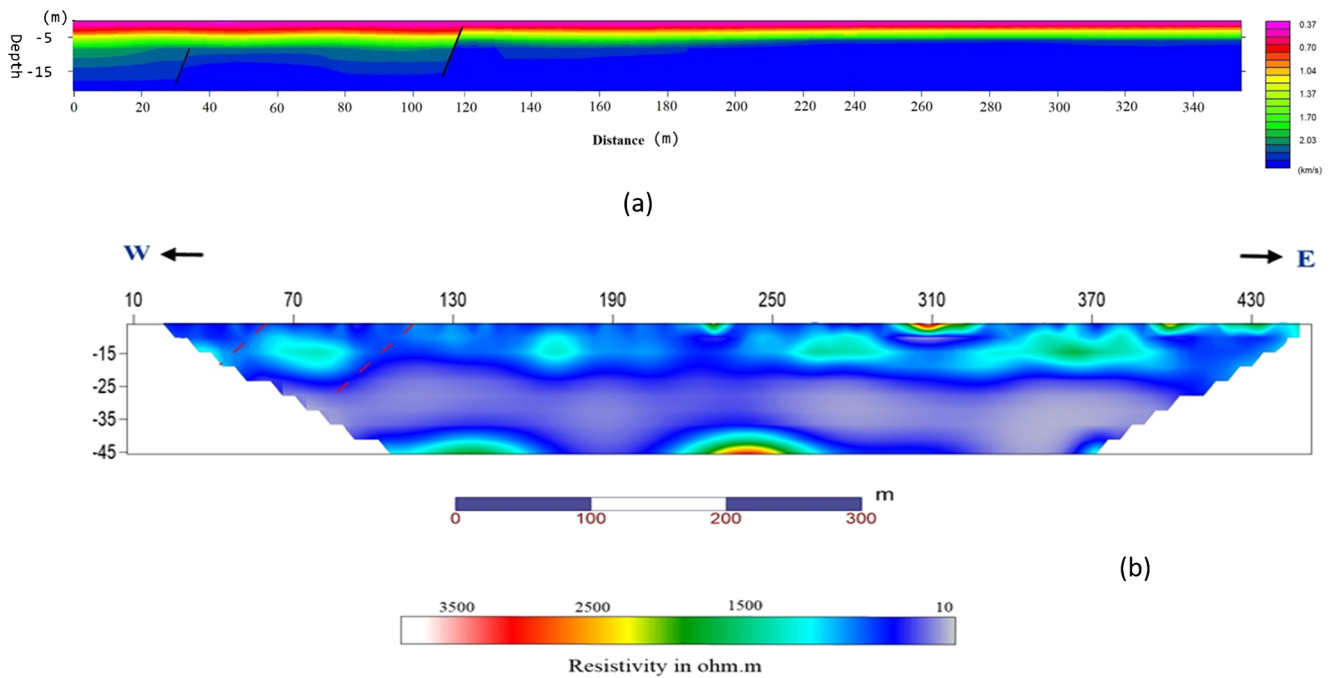


Fig. 6 P-wave 2D velocity- depth tomogram of line 2



**Fig. 7** The interpreted tomograms for the line1 from SRT and ERT data

## Conclusions

Depending on the results 2D ground models of both SRT and ERT, it is indicated that 1) the Qadimah fault in line 1 is indicated at distance of 120 m from the beginning of this line where an abrupt change in resistivity values along both sides

of this fault. Low resistivity values on the upper side of the fault might have been due to a salty brine channel just west of the reef complex, which is located to the far-right corner of Fig. 7. Additional possible fault has been identified at distance of 70 m was observed in resistivity tomography. A lower resistivity value was consistent with a channel of brine that

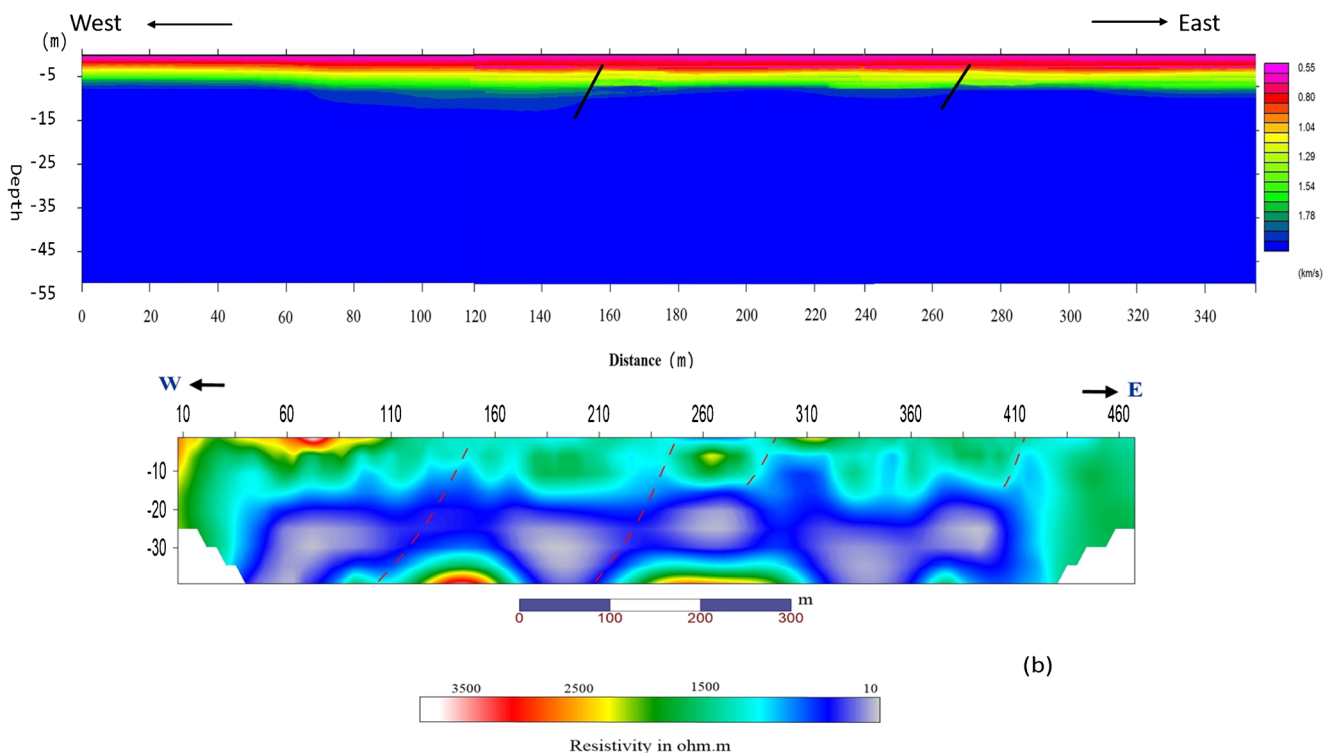


**Fig. 8** The interpreted tomograms for the line 2 from SRT and ERT data

is known to run parallel to the reef complex. Moreover, the deduced tomograms for the line 2 (Fig. 8) illustrate the presence of the Qadimah fault at distance of 150 m while another fault has been traced at distance of 260 m.

It is concluded that Qadimah active fault has been detected in the study area although its origin may be related to the continued extension of the rotated basement rocks or is controlled by salt tectonics (Smith 2012). Moreover, conjugate smaller faults have identified as well and extending parallel to this main Qadimah fault while others-oriented NNE to ENE. These results confirmed well with the detected Qadimah fault through the King Abdullah Economic City (KAEC) to the north of the studied area (AlTawash 2011). Installing earthquake local network equipped by global positioning system are highly recommended through the fault zone for earthquake hazard assessment and risk mitigation in Thuwal-Rabigh area.

**Acknowledgements** The authors thank the King Abdulaziz City for Science and Technology for contribution with field facilities. The authors would like to extend their sincere appreciation to the Deanship of Scientific Research at King Saud University for funding this research group (No. RGP-1436-010).

## Declarations

**Conflict of interest** The author(s) declare that they have no competing interests.

## References

- Aldridge DF, Oldenburg DW (1993) Two-dimensional tomographic inversion with finite-difference traveltimes. *J Seism Explor* 2:257–274
- AlTawash F (2011) Geophysical Imaging of Fault Structures over the Qadimah Fault. King Abdullah University of Science and Technology, Saudi Arabia
- Ammar AI, Kamal KA (2018) Resistivity method contribution in determining of fault zone and hydro-geophysical characteristics of carbonate aquifer, eastern desert, Egypt. *Appl Water Sci* 8:1. <https://doi.org/10.1007/s13201-017-0639-9>
- Ammon CJ, Vidale JE (1993) Tomography without rays. *Bull Seismol Soc Am* 83(2):509–528
- Fossen H (2010) Structural geology. Cambridge University Press
- Gilbert P (1972) Iterative methods for the three-dimensional reconstruction of an object from projections. *J Theor Biol* 36(1):105–117. [https://doi.org/10.1016/0022-5193\(72\)90180-4](https://doi.org/10.1016/0022-5193(72)90180-4)
- Giocoli A, Burrato P, Galli P, Lapenna V, Piscitelli S, Rizzo E, Romano G, Siniscalchi A, Magri C, Vannoli P (2008) Using the ERT method in tectonically active areas: hints from Southern Apennine (Italy). *Adv Geosci* 19:61–65
- Hanafy SM, Aboud E, Mesbah HSA (2012) Detection of subsurface faults with seismic and magnetic methods. *Arab J Geosci* 5(5): 1163–1172. <https://doi.org/10.1007/s12517-010-0255-6>
- Loke MH (1999) A Practical Guide to 2D and 3D Surveys. Electrical Imaging Surveys for Environmental and Engineering Studies, p 63. [www.abem.se](http://www.abem.se)
- Lutter D, Nowack R, Braile L (1990) Seismic imaging of upper crustal structure using travel times from the Passcal Ouachita experiment. *J Geophys Res* 95:4621–4631
- Mahmoud S. (2012) Detection of the Qademah Fault using Geophysical Methods. 7th Gulf Seismic Forum 2012, King Abdullah University of Science and Technology.
- Moore TA, Al-Rehaili MH (1989) Geologic Map of the Makkah Quadrangle, Sheet 21D, Kingdom of Saudi Arabia, Ministry of Petroleum and Mineral Resources, Deputy Ministry for Mineral Resources Publication, Jeddah, K.S.A
- Nemeth T, Normark E, Qin F (1997) Dynamic smoothing in crosswell traveltimes tomography. *Geophysics* 62(1):168–176
- Nolet G (1987) Seismic tomography: with applications in global seismology and exploration geophysics. D. Reidel Publishing Co., Dordrecht, Holland
- Park SK, and Wernicke B (2003) Electrical conductivity images of Quaternary faults and Tertiary detachments in the California Basin and Range, *Tectonics* V22, No. 4. <https://doi.org/10.1029/2001TC001324>
- Qin F, Luo Y, Olsen KB, Cai W, Schuster GT (1992) Finite-difference solution of the eikonal equation along expanding wavefronts. *Geophysics* 57(3):478–487
- Rezaei K (2016) Soil and Subsurface Sediment Microzonation Using with Seismic Refraction Tomography for Site Assessment (Case Study: IKIA Airport, Iran). *Open J Geol* 6(3):165–188. <https://doi.org/10.4236/ojg.2016.63016>
- Rinaldi VA, Ibarra HV, Viguera RF, and Harasimiuk JC (2019) Application of seismic tomography for detecting structural faults in a Tertiary Formation. *E3S Web of Conferences* 92, 18008. <https://doi.org/10.1051/e3sconf/20199218008>
- Rizzo E, Giampaolo V, Capozzoli L, and Grimaldi S (2019) Deep Electrical Resistivity Tomography for the Hydrogeological Setting of Muro Lucano Mounts Aquifer (Basilicata, Southern Italy). *Geofluids* Volume 2019, Article ID 6594983, 11 pages. <https://doi.org/10.1155/2019/6594983>
- Roobol MJ, Kadi KA (2008) Saudi Geological Survey Technical Report SGSTR-2008-6, 12. Saudi Geological Survey
- Skipwith P (1973) The Red Sea and coastal plain of the Kingdom of Saudi Arabia. Tech. Rec. T.R. 1973-1, Directorate General of Mineral Resources, Jeddah, Saudi Arabia, 149 pp.
- Smith RJ (2012) Investigation of the Qadimah Fault in Western Saudi Arabia using Satellite Radar Interferometry and Geomorphology Analysis Techniques. M.Sc. thesis, King Abdullah University of Science and Technology Thuwal, Kingdom of Saudi Arabia
- Zhu T, Feng R, Hao J, Zhou J, Wang H, Wang S (2009) The Application of Electrical Resistivity Tomography to Detecting a Buried Fault: A Case Study. *J Environ Eng Geophys* 14(3):145–151